

MNE: overparametrized neural evolution with applications to diffusion processes and sampling

Michael Lindsey
UC Berkeley and LBNL

Abstract

We propose a framework for solving evolution equations within parametric function classes, especially ones that are specified by neural networks. We call this framework the minimal neural evolution (MNE) because it is motivated by the goal of seeking the smallest instantaneous change in the neural network parameters that is compatible with exact solution of the evolution equation at a set of evolving collocation points. Formally, the MNE is quite similar to the recently introduced Neural Galerkin framework, but a difference in perspective motivates an alternative sketching procedure that effectively reduces the linear systems solved within the integrator to a size that is interpretable as an effective rank of the evolving neural tangent kernel, while maintaining a smooth evolution equation for the neural network parameters. We focus specifically on the application of this framework to diffusion processes, where the score function allows us to define intuitive dynamics for the collocation points. These can in turn be propagated jointly with the neural network parameters using a high-order adaptive integrator. In particular, we demonstrate how the Ornstein-Uhlenbeck diffusion process can be used for the task of sampling from a probability distribution given a formula for the density but no training data. This framework extends naturally to allow for conditional sampling and marginalization, and we show how to systematically remove the sampling bias due to parametric approximation error. We validate the efficiency, systematic improvability, and scalability of our approach on illustrative examples in low and high spatial dimensions.

1 Introduction

Neural network-based methods for solving differential equations, in both low and high spatial dimensions, are gaining increasing attention due to the capacity of neural network architectures to flexibly represent complicated functions. In particular, several frameworks have emerged for propagating neural network approximations in time. Though we do not attempt a comprehensive review, we point out that a contrast has emerged between global-in-time approaches and sequential-in-time approaches. The former category includes PINNS [39] among many other approaches. But our focus in this work is on the latter category, which includes Neural Galerkin schemes [11], regularized dynamical parametric approximation [19], TENG [13], and evolutionary deep neural networks [18], to name a few. For more comprehensive reviews, see, e.g., [11, 47, 6, 49].

Neural Galerkin schemes relate closely to optimization approaches based on natural gradients [2, 3, 38], including methods for optimizing quantum many-body wavefunctions within the Variational

Monte Carlo (VMC) framework [22, 5]. Wavefunction optimization based on natural gradients has a long history in the quantum chemistry literature, where it is known traditionally as stochastic reconfiguration (SR) [5]. Recently, a simple modification of stochastic reconfiguration called MinSR [12] and various extensions [21] have emerged as leading optimizers in VMC. Our work is motivated in part by the contrast in perspective between SR and MinSR.

Neural Galerkin and natural gradient approaches can be derived by projecting the dynamics that are prescribed in the function space onto the tangent space of the neural parametric manifold. At first glance, the natural gradient perspective suggests that it is desirable to take a large number N of sample points—in particular, a number greater than the number of neural network parameters p —in order to compute this projection accurately. Meanwhile, MinSR can be viewed as attempting to solve the prescribed dynamics exactly at a set of points, which in this work we interpret as collocation points. The philosophy of MinSR is that $p > N$, so that this prescription is underdetermined, and the *smallest* possible change to the neural network parameters is chosen among those that solve the dynamics exactly at the collocation points.

In fact, the SR and MinSR updates are mathematically equivalent, if the same regularization parameter is used for both methods [21], regardless of whether $p > N$ or $p < N$. (For SR, this regularization constitutes a shift of the metric. For MinSR, it softens the constraint at the collocation points.) Relatedly, it has been observed that in Neural Galerkin schemes, the parameter update minimizes a least squares objective [49], which corresponds to a soft version of the MinSR constraint. We point out that the impact of regularization on dynamical parametric approximation, including the Neural Galerkin framework, has been studied recently [19], though the focus of this work does not address the choice of collocation points.

Within Neural Galerkin schemes, key computational questions arise about how to deal with the least squares problems called as subroutines by the integrator, as well as how to integrate the parameter trajectories while simultaneously propagating the particles (which we will view as collocation points) to resolve the evolving neural state. Recent extensions of the basic Neural Galerkin framework have sought to address both points. First, the work [6] proposes sparse updates to the parameters at each time step. These updates can be viewed as projections onto a subspace of the neural tangent space. One drawback of this approach is that it relies on an incoherence assumption for the neural Jacobian. Moreover, due to the changing sparsity pattern of the update, the parameter dynamics cannot be viewed as smooth in time. Second, the work [47] has considered coupling the particle and parameter dynamics, with the goal of maintaining that the particles sample from an evolving sampling measure induced by the neural state. However, the approach in this work does not define a coupled system of smooth ODEs for the particles and parameters.

Our work seeks to address both of these computational questions. First, we propose an alternative approach to sketching the neural evolution based on a ridge regression perspective [35, 37]. This reduces the cost of the integrator from $O(pN^2)$ to $O(pN \log N + pn^2)$, where n is a sketch dimension that can be viewed as proportional (up to log factors) to the numerical rank of neural Jacobian. Importantly, we can use a fixed oblivious sketch matrix, allowing us to formulate smooth dynamics for the parameters that we call the minimal neural evolution (MNE).

To address the coupling of the parameter and collocation point dynamics, we focus specifically on applications to diffusion processes, where the score function [43] of the evolving state suggests an intuitive evolution of collocation points alongside the network parameters, similar to recent work on Fokker-Planck evolution [8, 9] which retrains neural network parameters at each time step,

rather than propagating them directly. By specifying joint smooth dynamics for the parameters and collocation points, we can leverage high-order adaptive integration methods for efficient and accurate propagation of both parameters and collocation points over time.

Interestingly, we do not encounter any analog of the tangent space collapse phenomenon [49] identified as a danger in Neural Galerkin schemes. Relatedly, we believe that further analysis of the generalization error of the MNE is an interesting topic for future study.

A key application of our work is to sampling problems, where MNE provides a method for generating samples from a probability distribution given its density function but no direct training data. In this setting, a natural *a priori* specification of the evolution of the collocation points is possible, further simplifying the integration.

A large body of recent work has focused on the application of ideas from generative modeling, powered by neural networks, to this sampling problem. We do not attempt a comprehensive review, but we refer to the recent work [1] for a thorough accounting and comparison of recent methods. We point out that many recent works such as Liouville flow [44], NETS [1], and AFT / CRAFT [4, 36] are based on the identification of an ‘annealing’ trajectory between the target density and an easier reference density, induced by linear interpolation of the log-densities. Others seek to freely optimize over density trajectories [17, 20, 48]. By contrast, our approach relies on the trajectory which connects the target density to a Gaussian distribution via Ornstein-Uhlenbeck diffusion, like diffusion models [42, 23, 43]. Relatedly, the recent work [46] also learns this trajectory, through alternative techniques.

One key advantage of the diffusion approach is that it allows for natural generalization to the task of conditional sampling and marginalization, which are of interest in many scientific applications, and can be similarly accommodated in generative models based on diffusion [25, 26, 24]. We illustrate our approach to these more general tasks and validate it with numerical experiments on a high-dimensional target distribution.

Unlike most other approaches to neural sampling, our approach to sampling relies on a preprocessing step where the target density is fit with a neural surrogate. Importantly, this preprocessing step does not rely on having exact samples from the target density. We believe that this could be an interesting starting point for other approaches as well. In particular, many target densities in Bayesian inference, which are of moderate dimension and therefore of particular interest as potential loci of ‘neural advantage’ in sampling (see, e.g., [28, 29, 14, 16, 15]), are characterized by extremely expensive density evaluations. For such distributions, relying on online density evaluations within a neural network training subroutine may be completely impractical, and training a neural surrogate on a limited set of representative collocation points (computed offline) may be a useful preprocessing step for other methods as well. (One of our example tasks in this work, sampling the Bayesian posterior for hyperparameters in Gaussian process regression [40, 33], can be viewed as such a problem. For large datasets, each density evaluation requires the evaluation of an expensive matrix determinant.)

Additionally, we extend our methodology to conditional sampling and marginalization, and we demonstrate how to systematically remove parametric approximation biases in the generated samples. We also demonstrate that the bias due to parametric approximation can be systematically removed from our samples (either full and conditional), similar to the recent work [1], via particle reweighting similar to diffusion Monte Carlo [5], with optional resampling to avoid population collapse.

To validate our approach, we present numerical experiments on a variety of diffusion-driven problems, including Langevin dynamics with nonequilibrium forcing, fully Bayesian Gaussian process regression, and sampling from an Allen-Cahn potential. These experiments demonstrate the effectiveness and scalability of MNE, showing that it can systematically improve solution accuracy while maintaining computational feasibility in high-dimensional settings.

This paper is structured as follows. In Section 2, we formalize the minimal neural evolution (MNE) framework. Section 3 presents the application of MNE to diffusion processes and, in turn, to sampling and marginalization. Section 4 provides numerical results demonstrating the accuracy and computational efficiency of the method.

Acknowledgments

This work was supported in part by a Sloan Research Fellowship and by the U.S. Department of Energy, Office of Science, Office of Advanced Scientific Computing Research’s Applied Mathematics Competitive Portfolios program under Contract No. AC02-05CH11231.

2 Minimal neural evolution

Consider a function evolution dictated by the equation

$$\partial_t u_t(x) = \mathcal{A}_t[u_t](x), \quad x \in \mathbb{R}^d, \quad (2.1)$$

where \mathcal{A}_t is an evolution operator that is possibly nonlinear and time-dependent.

Given a parametrization $u_\theta(x)$ of a function in terms of parameters $\theta \in \mathbb{R}^p$, we want to solve (2.1) within the parametric manifold $\{u_\theta : \theta \in \mathbb{R}^p\}$, or equivalently, seek an evolution for the parameters $\theta = \theta(t)$.

2.1 Preliminary derivation

To determine this evolution, we will insist that (2.1) is satisfied exactly at a collection of collocation points $X = (x_1, \dots, x_N)$, or almost exactly where a regularization parameter specifies the softness of these constraints. The collection $X = X(t)$ may be time-dependent with either a predetermined evolution or an evolution that is coupled to that of the parameters $\theta(t)$. We will use the notation $f(X) \in \mathbb{R}^N$ to denote the batched evaluation of a function $f : \mathbb{R}^d \rightarrow \mathbb{R}$ at all points in X . More generally, if $f(x)$ is vector-valued, then $f(X)$ will be matrix-valued with N columns.

Now for large overparametrized networks with $p \gg N$, the evolution of θ may be underspecified by the constraint at X . Therefore, for a small time increment, we propose to find the smallest change in the neural network parameters that is compatible with solving (2.1) at the collocation points.

Specifically, supposing that $\theta = \theta(t)$ is the current value of the parameters at some time t and $X = X(t)$ the current position of the collocation points, we seek to find the rate of change $\dot{\theta} = \dot{\theta}(t)$

for the parameters that satisfies:

$$\underset{\dot{\theta} \in \mathbb{R}^p}{\text{minimize}} \left\| [\nabla_{\theta} u_{\theta}(X)]^{\top} \dot{\theta} - \mathcal{A}_t[u_{\theta}](X) \right\|^2 + \lambda \|\dot{\theta}\|^2, \quad (2.2)$$

where $\|\cdot\|$ denotes the usual 2-norm and $\lambda > 0$ is a regularization parameter. Note that to derive this optimization problem we have used the chain rule $\frac{d}{dt} [u_{\theta(t)}(x)] = \langle \nabla_{\theta} u_{\theta(t)}(x), \dot{\theta}(t) \rangle$. For shorthand we will write

$$\Phi_{\theta}(x) = \nabla_{\theta} u_{\theta}(x), \quad (2.3)$$

which can be viewed as a feature map in the sense of the neural tangent kernel (NTK) [27].

Now the standard linear-algebraic manipulations for the ridge regression problem (2.2) reveal that the optimizer $\dot{\theta}$ is given by

$$\dot{\theta} = \Phi_{\theta}(X) [\Phi_{\theta}(X)^{\top} \Phi_{\theta}(X) + \lambda \mathbf{I}_p]^{-1} \mathcal{A}_t[u_{\theta}](X). \quad (2.4)$$

We can view (2.4) as an ODE specifying the evolution of $\theta(t)$. The evolution of $X(t)$ remains to be specified and the appropriate choice will be context-dependent, and we will discuss the choice below. Modulo this specification, as mentioned in the introduction, (2.4) can be viewed as a Neural Galerkin scheme [11] in which the same regularization parameter λ has been used to shift the metric.

Note that by comparing terms in (2.2), it makes sense to take

$$\lambda = N\varepsilon^2, \quad (2.5)$$

where $\varepsilon > 0$ roughly specifies an order of magnitude for the pointwise error tolerance.

Also observe that the matrix

$$K_{\theta}(X, X) := \Phi_{\theta}(X)^{\top} \Phi_{\theta}(X)$$

appearing in (2.4) is the kernel matrix of the NTK [27] evaluated on our collocation points. Modulo regularization, (2.4) seeks the update to the neural network parameters which is smallest in the sense of the NTK inner product while maintaining the evolution constraints at the collocation points. Note that this interpretation is not dependent on the evolution staying within some kernel learning regime [27].

2.2 Sketching

The matrix inversion required to implement (2.4) is $N \times N$, by contrast with the $p \times p$ matrix inversion that appears in the neural Galerkin method [11]—though, as mentioned above, this may alternatively be viewed as a least squares problem. In order to resolve the evolution with high fidelity throughout the spatial domain, it is of interest to enlarge the size N of the collocation set X as much as possible.

At the same time, enlarging this collocation set may introduce a significant amount of redundancy into the constraints due to rank deficiency of the NTK. This redundancy can be removed efficiently via a sketching procedure. Specifically, we will let $\Omega \in \mathbb{R}^{n \times N}$ denote a sketch matrix [35] which

reduces the dimension of a vector from N to n when multiplied from the left. Even more concretely, we consider as our sketch the subsampled randomized discrete Hartley transform, which is a partial isometry and is considered to be the best fast sketch for real matrices [35]:

$$\Omega v = \frac{1}{\sqrt{n}} [\operatorname{Re}(\mathbf{F}_N[\sigma \odot v]) - \operatorname{Im}(\mathbf{F}_N[\sigma \odot v])]_{\mathcal{I}}.$$

Here $\sigma \in \{\pm 1\}^N$ is a fixed vector of i.i.d. random signs, \mathbf{F}_N denotes the N -dimensional discrete Fourier transform, and \mathcal{I} is a fixed uniformly chosen random subset of $\{1, \dots, N\}$ of size n .

Then we can consider in place of (2.2) the sketched ridge regression problem

$$\underset{\dot{\theta} \in \mathbb{R}^p}{\text{minimize}} \left\| \Omega [\nabla_{\theta} u_{\theta}(X)]^{\top} \dot{\theta} - \Omega \mathcal{A}_t[u_{\theta}](X) \right\|^2 + \lambda \|\dot{\theta}\|^2, \quad (2.6)$$

which in turn yields

$$\dot{\theta} = \tilde{\Phi}_{\theta}(X) \left[\tilde{\Phi}_{\theta}(X)^{\top} \tilde{\Phi}_{\theta}(X) + \lambda \mathbf{I}_p \right]^{-1} \Omega \mathcal{A}_t[u_{\theta}](X), \quad (2.7)$$

where

$$\tilde{\Phi}_{\theta}(X) := \Phi_{\theta}(X) \Omega^{\top}.$$

Notably the cost of forming $\tilde{\Phi}_{\theta}(X)$ is only $O(pN \log N)$ and the total cost of implementing the right-hand side of the sketched MNE (2.7) is only

$$O(pN \log N + pn^2 + n^3),$$

where we recall that N is the number of collocation points, n is the sketch dimension, and p is the number of parameters. Typically a neural network ansatz will be overparametrized in the sense that the numerical rank of the NTK will be far smaller than p . Hence we can typically take $n < p$ (or even $n \ll p$) to be roughly on the order of the numerical rank of the NTK [35, 37].

We will fix a sketch matrix Ω throughout the dynamics, allowing us to view the right-hand side of (2.7) as a smooth, deterministic function of θ (and possibly X), so that standard solvers can be applied. In particular, we implement the ODE solver in JAX [10] using the Diffrax library [30]. We choose Tsitouras' 5/4 method [45] (i.e., `diffrax.Tsit5`) as our solver, which is an explicit Runge-Kutta method with adaptive time-stepping.

Subject to the specification of the dynamics of $X(t)$, we call (2.7) the *minimal neural evolution (MNE)*.

3 Application to diffusion processes

We will be interested in the density evolution induced by the stochastic differential equation [41]

$$dX_t = b_t(X_t) dt + \sigma \chi_{\mathcal{S}} \odot dB_t. \quad (3.1)$$

Here $b_t : \mathbb{R}^d \rightarrow \mathbb{R}^d$ is a time-dependent drift field, $\sigma > 0$ is a diffusion coefficient, and $\chi_{\mathcal{S}} = \sum_{i \in \mathcal{S}} e_i$ is a 'mask vector' which indicates the subset $\mathcal{S} \subset \{1, \dots, d\}$ of variables that are subject to diffusion. More general diffusion terms could be considered, but we restrict ourself to this case for simplicity since it covers all applications of interest below. Note with caution that throughout we will use the standard notation X_t for the SDE variable, but it should not be confused with our notation $X = X(t)$ for the collocation points.

3.1 General discussion

First we explain how the density evolution induced by (3.1) can be approached within the MNE framework.

To begin, observe that the Fokker-Planck equation [41] corresponding to (3.1) is given by

$$\partial_t \rho_t = -\nabla \cdot (\rho_t b_t) + \frac{\sigma^2}{2} \Delta_S \rho_t, \quad (3.2)$$

where $\Delta_S = \sum_{i \in \mathcal{S}} \frac{\partial^2}{\partial x_i^2}$ is a masked Laplacian.

We will not parametrize the evolution of ρ_t , but rather that of the energy function $u_t = -\log \rho_t$. By substitution and repeated application of the chain rule, one deduces the following evolution equation for u_t :

$$\partial_t u_t = \nabla \cdot b_t - b_t \cdot \nabla u_t + \frac{\sigma^2}{2} \Delta_S u_t - \frac{\sigma^2}{2} |\nabla_S u_t|^2, \quad (3.3)$$

where $\nabla_S := \left(\frac{\partial}{\partial x_i} \right)_{i \in \mathcal{S}}$ denotes the masked gradient.

Then we can directly apply MNE to the operator

$$\mathcal{A}_t[u] = \nabla \cdot b_t - b_t \cdot \nabla u + \frac{\sigma^2}{2} \Delta_S u - \frac{\sigma^2}{2} |\nabla_S u|^2. \quad (3.4)$$

We would like to insist that the collocation points $X(t)$ evolve with the density. To initialize them, we might choose $X(0)$ to be samples from ρ_0 . However, the consistency of the scheme does not require us to do so exactly. Either way, it is natural to demand that $X(t)$ evolve according to a deterministic flow that implements the density evolution.

Since the Fokker-Planck equation can be viewed as a transport equation

$$\partial_t \rho_t = -\nabla \cdot \left(\rho_t \left[b_t + \frac{\sigma^2}{2} \chi_S \odot \nabla u_t \right] \right)$$

with drift field $b_t + \frac{\sigma^2}{2} \chi_S \odot \nabla u_t$, we can impose the following evolution for the collocation points:

$$\dot{X} = b_t(X) + \frac{\sigma^2}{2} \chi_S \odot \nabla u_\theta(X),$$

where the entrywise product is broadcasted suitably. Together with equation (2.7) for $\dot{\theta}$, this completes the specification of a system of ODEs for $(\theta(t), X(t))$.

However, in the application of MNE to marginalization and sampling considered below, we will consider an alternative (*a priori*) specification of $X(t)$ which need not be solved for jointly with $\theta(t)$.

3.2 Sampling and marginalization

We can apply the density evolution framework of the preceding Section 3.1 to the problem of sampling a probability density

$$\rho(x) \propto e^{-u(x)},$$

where $u(x)$ is known.

Our approach also allows for marginal estimation and conditional sampling. Specifically, for any subset of variables $\mathcal{S} \subset \{1, \dots, d\}$, let \mathcal{S}' denote its complement, and identify $x = (x_{\mathcal{S}}, x_{\mathcal{S}'})$ in the notation, assuming for simplicity that the variables have been so ordered. Then let

$$\rho_{\mathcal{S}'}(x_{\mathcal{S}'}) := \int_{\mathbb{R}^{|\mathcal{S}|}} \rho(x) dx_{\mathcal{S}}$$

denote the marginal density. We will show how to construct an approximation of the marginal energy function $u_{\mathcal{S}'}$ which is defined up to a constant shift by

$$\rho_{\mathcal{S}'}(x_{\mathcal{S}'}) \propto e^{-u_{\mathcal{S}'}(x_{\mathcal{S}'})}.$$

Moreover let

$$\rho(x_{\mathcal{S}} | x_{\mathcal{S}'}) = \frac{\rho(x)}{\rho_{\mathcal{S}'}(x_{\mathcal{S}'})}$$

denote the conditional density for the variables in \mathcal{S} given those in \mathcal{S}' . We will show how to draw samples $x_{\mathcal{S}}$ from this distribution for arbitrary given $x_{\mathcal{S}'}$. In particular, we will show how the bias due to our parametric approximations can be systematically removed from these samples. Note that in the special case $\mathcal{S} = \{1, \dots, d\}$, we recover the capacity to draw samples from the full target distribution ρ .

3.2.1 Preprocessing

As a first step, we obtain some initial collocation points $X_{\text{init}} = (x_1, \dots, x_N)$ adapted to the target density ρ . Importantly, we do not need to insist that X_{init} consists of samples from ρ . Instead, we can always obtain X_{init} by running a few iterations of a Markov chain Monte Carlo (MCMC) sampler with respect to the target density, so that X_{init} attains coverage of the ‘typical set’ [7] of ρ . For example, even if multimodality prevents rapid mixing of MCMC, it is not necessarily a problem if the initial samples X_{init} exhibit an improper balance between modes, as long as all modes are represented.

The next step is to fit u with a neural network surrogate $u_{\theta_{\text{init}}}$ on our initial collocation points. We achieve this by minimizing the error of the score function on our collocation points

$$\mathcal{L}(\theta) = \frac{1}{N} \sum_{i=1}^N |\nabla u_{\theta}(x_i) - \nabla u(x_i)|^2, \quad (3.5)$$

i.e., setting $\theta_{\text{init}} = \underset{\theta \in \mathbb{R}^p}{\text{argmin}} \mathcal{L}(\theta)$.

3.2.2 MNE specification

In the context of the general presentation in Section 3.1 we make the choice

$$b_t(x) = -\gamma \chi_{\mathcal{S}} \odot x \quad (3.6)$$

for the drift field, where $\gamma > 0$ is a damping parameter. Then the operator $\mathcal{A} = \mathcal{A}_t$ specified by (3.4) is time-independent.

For this choice of b_t , the density ρ_t for the diffusion process (3.1)-(3.2) converges rapidly to the product density

$$\rho_\infty(x) \propto e^{-\frac{1}{\sigma^2/\gamma} \|x_S\|^2} \rho_{S'}(x_{S'}),$$

i.e., the product of the marginal density $\rho_{S'}$ for the variables in S' with a normal distribution $\mathcal{N}\left(0, \frac{\sigma^2}{2\gamma} \mathbf{I}_{|S|}\right)$ for the variables in S .

Since the dynamics become smoother at larger times, we introduce the time change $t(s) = \frac{1}{2}s^2$ and evolve with respect to the transformed variable s , defining $\tilde{u}_s = u_{t(s)}$. Then by the chain rule, together with (3.3)-(3.4), we have that

$$\partial_s \tilde{u}_s(x) = s\mathcal{A}[\tilde{u}_s](x), \quad (3.7)$$

and we can apply the MNE induced by the choice of operator $\tilde{\mathcal{A}}_s[u] = s\mathcal{A}[u]$ to implement the evolution of \tilde{u}_s in the transformed time variable s , deducing an evolution of parameters $\theta(s)$ such that $\tilde{u}_s \approx u_{\theta(s)}$. We choose $\theta(0) = \theta_{\text{init}}$ as our initial condition, where θ_{init} consists of the parameters of our surrogate model as computed in Section 3.2.1.

Then we view $u_0 = u_{\theta(0)}$ as the exact initial condition for our dynamics (3.7). We will let

$$\rho_s(x) \propto e^{-\tilde{u}_s(x)}$$

denote the density induced by \tilde{u}_s over the course of the exact evolution (3.7), and we will overload the notation ρ_s to indicate corresponding conditional distributions as well, as shall be clear from context.

3.2.3 Collocation points

With initial collocation points X_{init} obtained as specified in Section 3.2.1, we obtain a trajectory $X(t)$ via the formula

$$X(t) = (\mathbf{1} - \chi_S) \odot X_{\text{init}} + \chi_S \odot \left[e^{-\gamma t} X_{\text{init}} + \sqrt{\frac{\sigma^2}{2\gamma} (1 - e^{-2\gamma t})} Z \right], \quad (3.8)$$

where the columns of $Z = (z_1, \dots, z_N)$ are i.i.d. samples from $\mathcal{N}(0, \mathbf{I}_d)$. Note that only the variables in S are changing over this trajectory.

The trajectory (3.8) is chosen so that if the columns of X_{init} are drawn from some initial sampling density ρ_{init} (which need not coincide with the target density ρ), then the columns of $X(t)$ sample exactly from the density obtained by propagating ρ_{init} according to the Fokker-Planck evolution specified by our drift (3.6) up to time t . Importantly, the dependence of $X(t)$ on t is smooth, and by contrast it is undesirable to produce a trajectory by solving the SDE (3.1). The same type of sample trajectory is commonly used for training score-based diffusion models [43].

More properly, after the time change to s via $t(s) = \frac{1}{2}s^2$, we choose $\tilde{X}(s) = X(t(s))$ as our set of evolving collocation points.

3.2.4 Marginalization

Note that if $|\mathcal{S}| < n$, then we can deduce the energy function $u_{\mathcal{S}'}$ of the marginal distribution $\rho_{\mathcal{S}'} \propto e^{-u_{\mathcal{S}'}}$ via the evaluation

$$u_{\mathcal{S}'}(x_{\mathcal{S}'}) := u_{\infty}(0, x_{\mathcal{S}'}).$$

In practice we approximate $u_{\infty} \approx u_{\theta(s_f)}$, where s_f is the final time of our evolution.

3.2.5 Sampling

We can use the learned MNE to draw samples $x_{\mathcal{S}}$ from the conditional distribution $\rho(\cdot | x_{\mathcal{S}'})$, for arbitrary given $x_{\mathcal{S}'}$. In the case where $\mathcal{S} = \{1, \dots, d\}$, we simply draw samples from the full distribution ρ .

To achieve this, consider the reverse diffusion [43]:

$$dX_s = (s_f - s) \chi_{\mathcal{S}} \odot [\gamma X_s - \sigma^2 \nabla \tilde{u}_{s_f - s}(X_s)] ds + (s_f - s)^{1/2} \sigma \chi_{\mathcal{S}} \odot dB_s, \quad s \in [0, s_f]. \quad (3.9)$$

Again note with caution that we use the standard notation X_t for the SDE variable, but it should not be confused with our notation $X = X(t)$ for the collocation points.

The Fokker-Planck evolution of (3.9) reverses the Fokker-Planck evolution (3.2) of the forward diffusion (3.1), taking into account the time change $t = t(s)$, and therefore if $X_0 \sim \rho_{s_f}$ then $X_{s_f} \sim \rho_0$.

Since these dynamics leave the variables in \mathcal{S}' unaltered, we can alternatively consider the simpler dynamics for the remaining variables $Y_s = [X_s]_{\mathcal{S}}$:

$$dY_s = (s_f - s) [\gamma Y_s - \sigma^2 \nabla_{\mathcal{S}} \tilde{u}_{s_f - s}(Y_s, x_{\mathcal{S}'})] ds + (s_f - s)^{1/2} \sigma dB_s, \quad s \in [0, s_f], \quad (3.10)$$

where by some abuse of notation B_s here indicates a Brownian motion of dimension $|\mathcal{S}|$. This diffusion must transport the conditional distribution $\rho_{s_f}(\cdot | x_{\mathcal{S}'})$ to $\rho_0(\cdot | x_{\mathcal{S}'})$ for any given $x_{\mathcal{S}'}$.

Under the assumption that s_f is sufficiently large, we have that the law of the conditional distribution $\rho_{s_f}(\cdot | x_{\mathcal{S}'})$ is approximately $\mathcal{N}\left(0, \frac{\sigma^2}{2\gamma} \mathbf{I}_{|\mathcal{S}|}\right)$, independent of $x_{\mathcal{S}'}$. Moreover, $\rho_0(\cdot | x_{\mathcal{S}'}) \approx \rho(\cdot | x_{\mathcal{S}'})$, provided that our initial condition $\tilde{u}_0 = u_{\theta(0)}$ for the MNE approximates the target energy function u .

Therefore, to draw an approximate sample y from the conditional distribution $\rho(\cdot | x_{1:d'})$, we would like to draw $Y_0 \sim \mathcal{N}\left(0, \frac{\sigma^2}{2\gamma} \mathbf{I}_{|\mathcal{S}|}\right)$ and then solve the SDE (3.10) to obtain our sample as Y_{s_f} . However, since we do not have access to the exact evolution \tilde{u}_s but rather only our neural approximation $u_{\theta(s)}$, we instead obtain our sample by solving, obtained from (3.10) via this substitution:

$$dY_s = (s_f - s) [\gamma Y_s - \sigma^2 \nabla_{\mathcal{S}} u_{\theta(s_f - s)}(Y_s, x_{\mathcal{S}'})] ds + (s_f - s)^{1/2} \sigma dB_s, \quad s \in [0, s_f]. \quad (3.11)$$

3.2.6 Unbiasing

There are several sources of bias in the sampling procedure described above due to the parametric approximation error both of the initial condition $u_{\theta(0)} \approx u$ and the evolution itself. All of these can be systematically removed.

Note that if the MNE dynamics $u_{\theta(s)}$ were to exactly satisfy (3.7), and if Y_0 was drawn exactly from $\rho_{s_f}(\cdot | x_{S'})$, then Y_s computed via (3.11) would be an exact sample from $\rho_{s_f-s}(\cdot | x_{S'})$ for all $s \in [0, s_f]$. More generally, we can use the discrepancy by which the equality (3.7) fails to hold to evolve weights for our samples. The same idea has also appeared in the recent work [1].

To wit, we couple the SDE (3.10) for Y_s to an evolution for the log-weight of the sample

$$\dot{w}(s) = (s_f - s)\mathcal{A}[u_{\theta(s_f-s)}](Y_s, x_{S'}) + \frac{d}{ds}u_{\theta(s_f-s)}(Y_s, x_{S'}), \quad (3.12)$$

where $w(0) = 0$. In so doing we can obtain a weighted sample $(y, w) = (Y_{s_f}, w(s_f))$. Repeating this procedure M times in parallel we can obtain a collection of weighted samples $(y^{(i)}, w^{(i)})_{i=1}^M$, from which empirical estimates according to the conditional distribution $\rho_0(\cdot | x_{S'})$ can be estimated using the weighted empirical measure

$$\frac{\sum_{i=1}^M e^{w^{(i)}} \delta_{y^{(i)}}}{\sum_{i=1}^M e^{w^{(i)}}}. \quad (3.13)$$

During the propagation, if the effective sample size [34] of the weighted ensemble drops below αM for some parameter $\alpha \in (0, 1)$, we can perform unbiased resampling to avoid population collapse. Although we have implemented and validated this capacity, we never need to rely on it in our experiments reported below. In principle, MCMC steps with respect to the target $e^{-u_{\theta(s_f-s)}}$ could also be included after resampling, as is done in several recent works [4, 36].

Finally, we must address the bias due to the facts that (1) the law of $\rho_{s_f}(\cdot | x_{S'})$ is not exactly $\mathcal{N}\left(0, \frac{\sigma^2}{2\gamma}\mathbf{I}_{|S|}\right)$, i.e., Y_0 is not exactly drawn from $\rho_{s_f}(\cdot | x_{S'})$, and (2) the law of $\rho_0(\cdot | x_{S'})$ is not exactly $\rho(\cdot | x_{S'})$. We can address both issues by importance sampling.

To wit, after drawing $Y_0 \sim \mathcal{N}\left(0, \frac{\sigma^2}{2\gamma}\mathbf{I}_{|S|}\right)$, we can initialize

$$w(0) = \frac{\gamma}{\sigma^2}\|Y_0\|^2 - u_{s_f}(Y_0, x_{S'})$$

for joint dynamics of $(Y_s, w(s))$ specified by (3.11) and (3.12). Then after solving these dynamics up to time s_f , we endow our sample $y = Y_{s_f}$ with the modified weight

$$w = w(s_f) + u_{s_f}(Y_{s_f}, x_{S'}) - u(Y_{s_f}, x_{S'}).$$

Again, we may repeat this procedure in parallel to draw many weighted samples $(y^{(i)}, w^{(i)})_{i=1}^M$ and estimate expectations using the weighted empirical measure (3.13).

4 Numerical experiments

Now we describe several numerical experiments validating the MNE framework for Fokker-Planck evolution and conditional sampling. Our implementation is in JAX [10] with double precision, and to solve ODEs we use the Diffrax library [30]. As mentioned above we choose Tsitouras' 5/4 method [45] (i.e., `diffrax.Tsit5`) as our solver, which is an explicit Runge-Kutta method with adaptive time-stepping, using relative and absolute tolerances of 10^{-3} and 10^{-6} , respectively. All

experiments were run on a single A100 GPU. The cost of running the ODE solver for the MNE is the main computational cost of our methodology. Each such solve needed in Section 4.1 below was completed in about 30 seconds or below. Each such solve needed in Sections 4.2 and 4.3 was completed in about 10 seconds or below.

4.1 Langevin dynamics with nonequilibrium forcing

We consider the diffusion induced by the following SDE

$$\begin{cases} dQ_t = P_t dt \\ dP_t = F_t(Q_t) dt + \sigma dB_t, \end{cases}$$

which are the underdamped Langevin dynamics for a particle with unit mass, time-dependent force term $q \mapsto F_t(q)$, and diffusion coefficient σ . The standard form (3.1) can be recovered by viewing $X_t = (Q_t, P_t)$ and $x = (q, p)$.

As an illustrative example for the MNE we consider the case of $x \in \mathbb{R}^{1+1}$ with forcing specified by

$$F_t(q) = -q + e^{-q^2/2} \cos(t)$$

and $\sigma = 0.1$.

The Fokker-Planck equation (3.2) is solved using the MNE approach of Section 2, including the strategy for evolving the collocation point positions $X(t)$. For our parametrization $\theta \mapsto u_\theta$ we use a MLP architecture with two hidden layers of width 128 and cosine activations.

We take the Gaussian initial condition

$$u_0 = \frac{1}{2} [(q-1)^2 + p^2],$$

and to construct $X(0)$ we simply draw $N = 10^4$ samples from $\rho_0 \propto e^{-u_0}$.

To initialize the MNE we must find parameters $\theta(0)$ such that $u_{\theta(0)} \approx u_0$. We achieve this by optimizing the score-matching objective (3.5) using the Adam optimizer [32] with default parameters and learning rate 10^{-2} . For this example, since it is possible to fit to a high accuracy, the initial fit error is ignored and we simply treat $u_{\theta(0)}$ as the exact initial condition of the dynamics (3.3).

Illustrative snapshots of the density evolution and particle trajectories $X(t)$ are shown in Figure 4.1 for several times in the range $t \in [0, 30]$. These were obtained with regularization parameter $\varepsilon = 10^{-6}$ (cf. (2.5)) and sketch dimension $n = 800$. We will validate the accuracy for these choices below. Animated GIFs of the evolution are available at

quantumtative.github.io/mne

To demonstrate the systematic improvability of the method we plot the size of the residual for solving (3.3), aggregated in the root mean square (RMS) sense over the evolving set collocation points (cf. (2.2)):

$$r(t) = \frac{1}{\sqrt{N}} \left\| [\nabla_\theta u_\theta(X(t))]^\top \dot{\theta}(t) - \mathcal{A}_t[u_\theta](X(t)) \right\|, \quad (4.1)$$

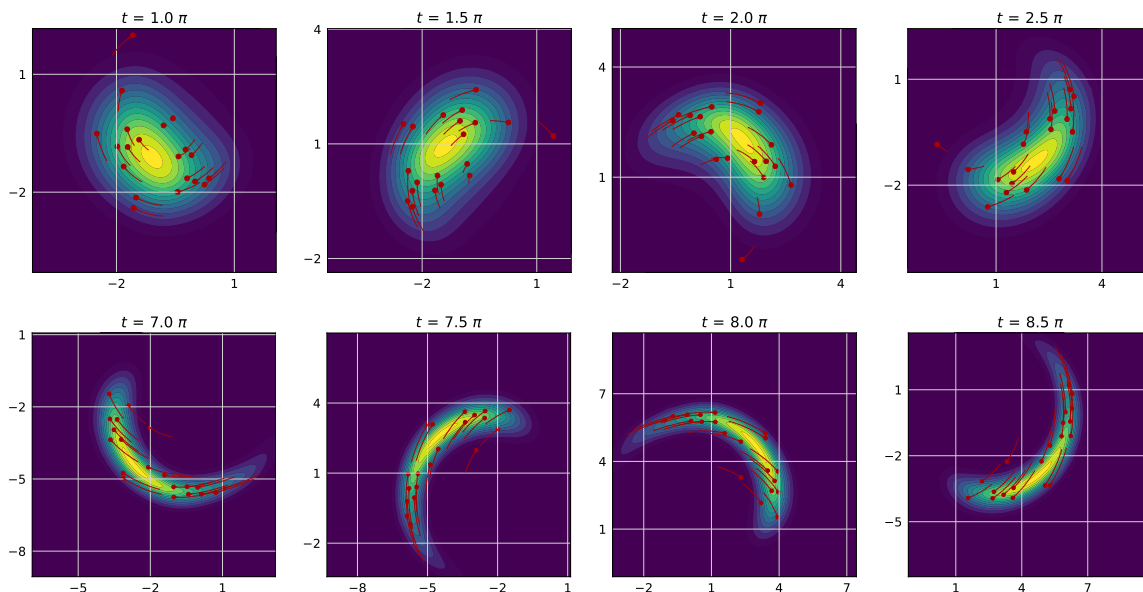


Figure 4.1: RMS residual (4.1) over the MNE trajectory for the example described in Section 4.1, plotted for various choices of the tolerance ε (cf. (2.5)). The sketch dimension is $n = 700$ for each curve.

for several values of the sketch dimension n and regularization parameter ε in Figures 4.2 and 4.3, respectively. Note that accuracy for our parametrization saturates by about $n = 600$. Moreover, past about $\varepsilon = 10^{-6}$, the MNE for this parametrization fails to generalize outside the collocation points and the ODE solver becomes unstable.

Figures 4.2 and 4.3 validate the systematic improvability of the methodology up to the accuracy allowed by the parametrization, consistent with prior expectations. Note that the experiments can be viewed as revealing a numerical rank for the MNE that is far smaller than the number of parameters.

4.2 Bayesian inverse problem

We will apply the MNE to sample from the Bayesian posterior distribution in a fully Bayesian Gaussian process regression (GPR) problem. For further background, see, e.g., [31]. This experiment can be viewed as an application of the techniques of Section 3.2, where we choose $\sigma = \sqrt{2}$ and $\gamma = 1$.

We construct a dataset of ordered pairs (t_i, y_i) , $i = 1, \dots, m$, as

$$y_i = f(t_i) + \epsilon_i,$$

where $\epsilon_i \sim \mathcal{N}(0, 0.1^2)$ are i.i.d. (Here ‘ t ’ does not indicate a time variable in the sense of our diffusion process, but rather an independent regression variable.) In our experiments, we draw the t_i independently from the uniform distribution over $[-1, 1]$. We also choose $f(t) = \sin(5t)$ and $m = 20$.

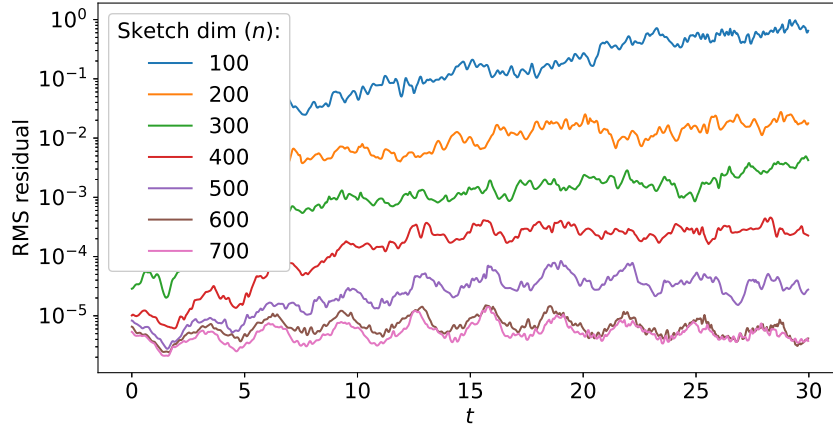


Figure 4.2: RMS residual (4.1) over the MNE trajectory for the example described in Section 4.1, plotted for various choices of the sketch dimension n . The regularization parameter is $\varepsilon = 10^{-6}$ for each curve.

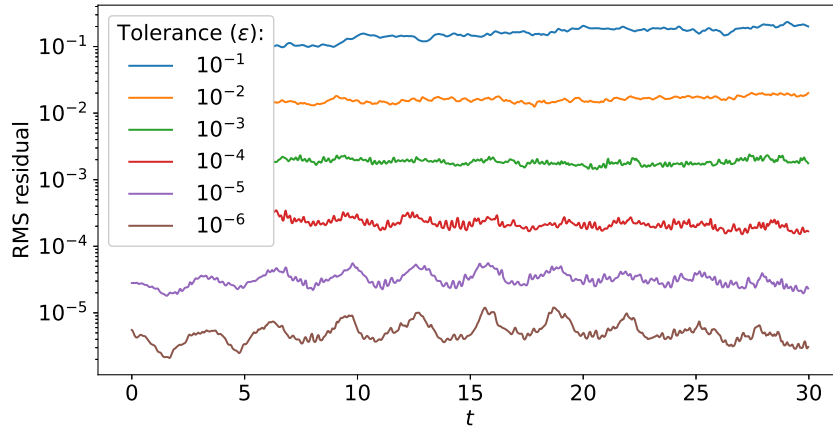


Figure 4.3: RMS residual (4.1) over the MNE trajectory for the example described in Section 4.1, plotted for various choices of the tolerance ε (cf. (2.5)). The sketch dimension is $n = 700$ for each curve.

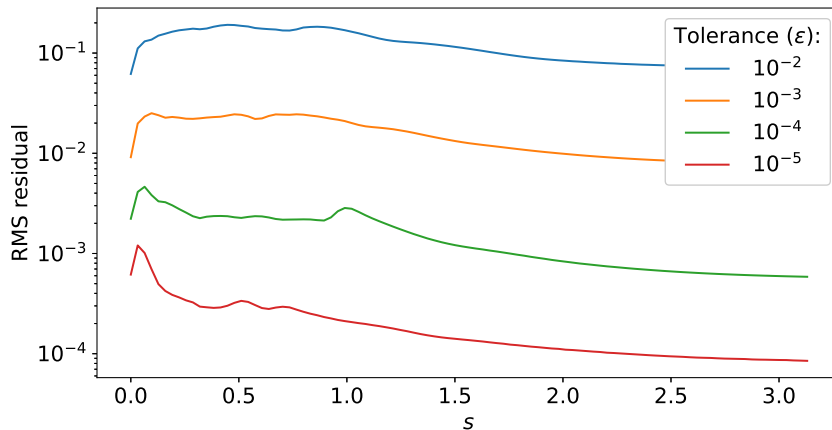


Figure 4.4: RMS residual (4.1) over the MNE trajectory for the example described in Section 4.2, plotted for various choices of the tolerance ε (cf. (2.5)). The sketch dimension is $n = 700$ for each curve.

For our GPR, we consider the exponential kernel

$$\Sigma(t_1, t_2) = \alpha^2 e^{-\frac{(t_1 - t_2)^2}{\rho^2}},$$

where $\alpha > 0$ and $\rho > 0$ indicate hyperparameters for the vertical and horizontal scales of the function. Moreover, we let $\sigma > 0$ denote a hyperparameter for the unknown standard deviation of the noise.

We will write $\alpha = e^{x_1}$, $\rho = e^{x_2}$, and σ^{x_3} in terms of hyperparameters $x = (x_1, x_2, x_3)$ to be inferred. As a prior over x we take the standard normal distribution $p(x) \propto e^{-\|x\|^2/2}$. Then the posterior distribution for x , given our observations y_i , is specified by the energy function

$$u(x) = \frac{1}{2} \log \det \mathbf{K}(x) + \frac{1}{2} y^\top \mathbf{K}(x)^{-1} y - \log p(x),$$

which we view as specifying our target for sampling.

To fit our surrogate model, we pick the initial collocation points by running 1000 iterations of the Metropolis-adjusted Langevin algorithm (MALA) with step size 0.02 on an ensemble of $N = 10^4$ walkers initialized at the origin in \mathbb{R}^3 . For our neural network parametrization we use the MLP architecture with 2 hidden layers of width 128 and softplus activations. We fit the surrogate model with Adam [32] using standard hyperparameters and learning rate 4×10^{-4} .

We take $s_{\max} = \sqrt{10}$ to be the final time for the MNE. In Figure 4.4 we plot the appropriate RMS residual (cf. (4.1)) for this problem as a function of time, for a fixed sketch dimension $n = 700$ and several values of the regularization parameter ε .

The results once again validate the systematic improvability of the approach.

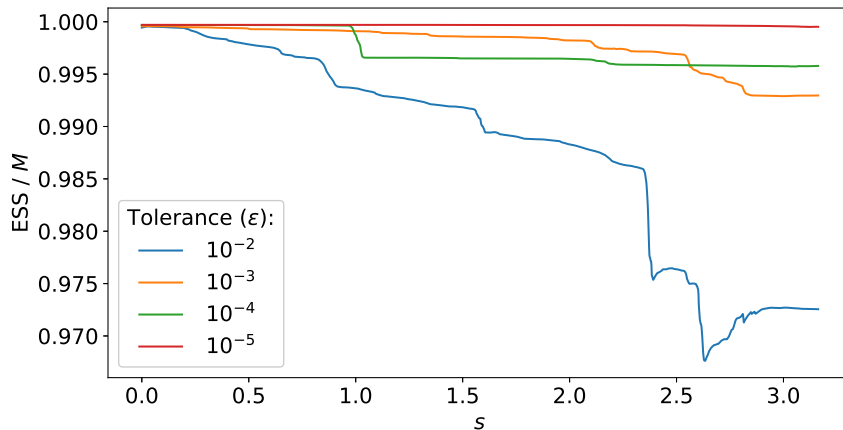


Figure 4.5: ESS per sample for the evolving weighted ensemble of $M = 10^4$ samples over the reverse diffusion trajectory for the example described in Section 4.2, plotted for various choices of the tolerance ε (cf. (2.5)). The sketch dimension is $n = 700$ throughout.

Then we use the learned trajectory $\theta(s)$ from each of these experiments to draw an unbiased weighted ensemble of $M = 10^4$ samples from $e^{-u_{\theta(s_{\max}-s)}}$, evolving with $s \in [0, s_{\max}]$, following the approach of Section 3.2.6. To solve the SDE (3.11), we use the Euler-Maruyama method with step size $s_{\max}/2000$. The ESS [34] per sample is plotted in Figure 4.5 over the course of the ensemble trajectory. In particular, the samples are weighted at $s = 0$ according to the initial step of the unbiasing procedure of Section 3.2.6. The unbiasing step at the end is ignored here because its impact is negligible, due to the excellent fit of the surrogate model.

4.3 Allen-Cahn potential

Finally, we consider the high-dimensional distribution induced by the Allen-Cahn potential for a 1-dimensional field with periodic boundary condition:

$$u(x) = \frac{\beta}{2} \sum_{i=0}^{d-1} \left[\left(\frac{x_{i+1} - x_i}{h} \right)^2 + (x_i^2 - 1)^2 \right].$$

The entries of x are zero-indexed with the convention that $x_d = x_0$. Here $h > 0$ is a spatial grid size parameter and $\beta > 0$ is an inverse temperature. We choose $d = 20$, $h = 1/20$, and $\beta = 0.3$. This choice of parameters exhibits bimodality in the distribution $\rho \propto e^{-u}$. In particular the modes are centered at $x = \pm 1$. This experiment can be viewed as an application of the techniques of Section 3.2, where we choose $\sigma = \sqrt{2}$ and $\gamma = 1$.

To fit our surrogate model, we pick the initial collocation points by running 4000 iterations of MALA with step size 10^{-3} on an ensemble of $N = 10^4$ walkers initialized according to the standard normal distribution on \mathbb{R}^d . We comment that this ensemble is *far* from fully mixed with respect to

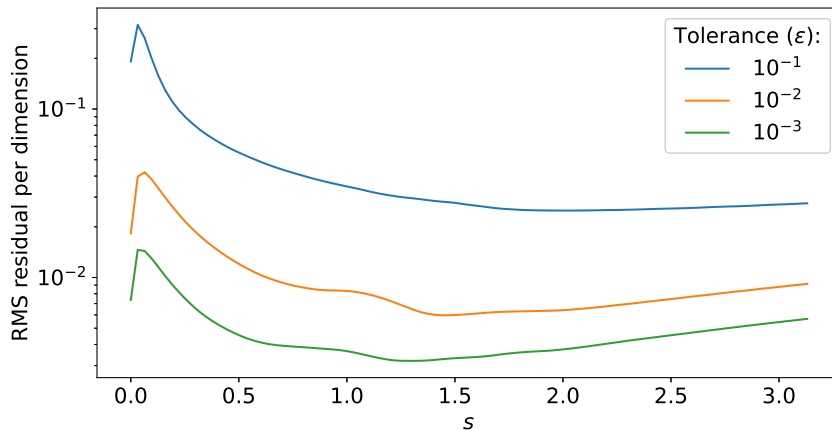


Figure 4.6: RMS residual (4.1) over the MNE trajectory for the example described in Section 4.3, plotted for various choices of the tolerance ε (cf. (2.5)). The sketch dimension is $n = 2000$ for each curve.

the target density ρ . For our neural network parametrization we use the MLP architecture with 2 hidden layers of width 128 and softplus activations. We fit the surrogate model with Adam using standard hyperparameters and learning rate 10^{-4} .

We take $s_{\max} = \sqrt{10}$ to be the final time for the MNE. In Figure 4.6 we plot the appropriate RMS residual (cf. (4.1)) for this problem as a function of time, for a fixed sketch dimension $n = 2000$ and several values of the regularization parameter ε .

Then we use the learned trajectory $\theta(s)$ from each of these experiments to draw an unbiased weighted ensemble of $M = 10^4$ samples from $e^{-u_{\theta}(s_{\max}-s)}$, evolving with $s \in [0, s_{\max}]$, following the approach of Section 3.2.6. To solve the SDE (3.11), we use the Euler-Maruyama method with step size $s_{\max}/2000$. The ESS per sample is plotted in Figure 4.7 over the course of the ensemble trajectory. In particular, the samples are weighted at $s = 0$ according to the initial step of the unbiasing procedure of Section 3.2.6. The final ESS values after the unbiasing step at the end of the reverse diffusion are reported in the caption of Figure 4.7.

Finally, we apply the MNE to conditional sampling, choosing $\mathcal{S} = \{1, \dots, d-1\}$ (i.e., leaving out the zeroth index) in the notation of Section 3.2 and conditioning on $x_0 = 1$, which essentially confines us to a single mode of the bimodal distribution. The setup for this experiment is the same as in the preceding discussion. In Figure 4.8 we plot the appropriate RMS residual (cf. (4.1)) for this problem as a function of time.

The ESS plot analogous to Figure 4.7 is qualitatively quite similar for this case of conditional sampling. Thus we omit the plot, but we include the final ESS values in the caption of Figure 4.8, which are quite similar to those obtained in the full sampling case.

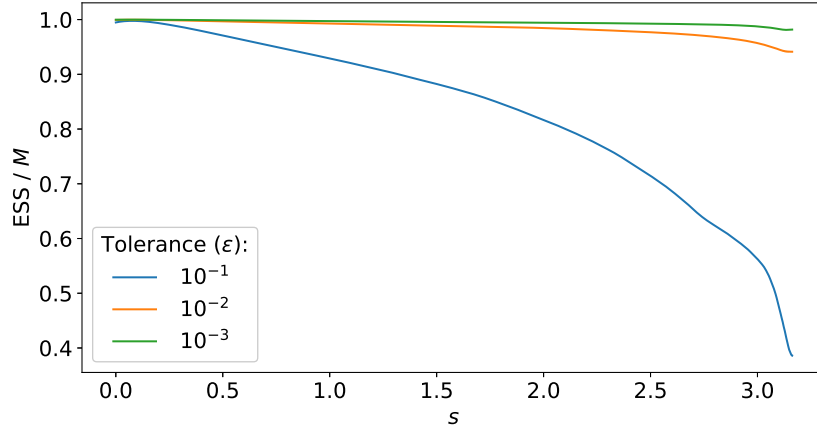


Figure 4.7: ESS per sample for the evolving weighted ensemble of $M = 10^4$ samples over the reverse diffusion trajectory for the example described in Section 4.3, plotted for various choices of the tolerance ε (cf. (2.5)). The sketch dimension is $n = 2000$ throughout. The final values of the ESS per sample after the unbiasing step at the end of the reverse diffusion are 0.386, 0.937, and 0.978 for $\varepsilon = 10^{-1}$, 10^{-2} , and 10^{-3} , respectively.

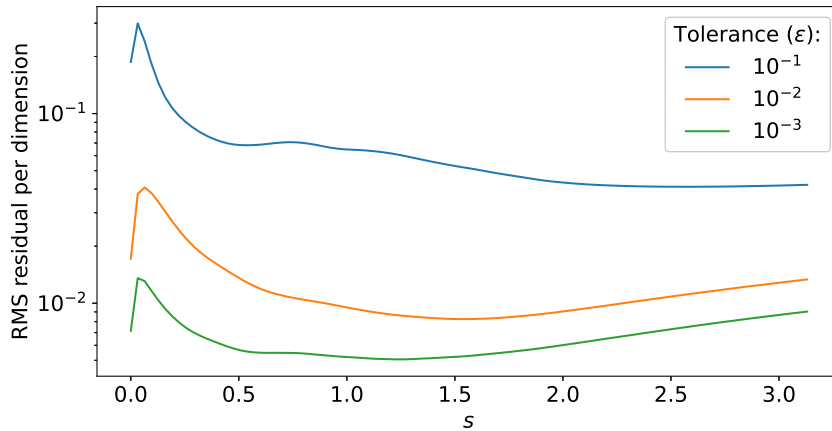


Figure 4.8: RMS residual (4.1) over the MNE trajectory for the example described in Section 4.3 with $\mathcal{S} = \{1, \dots, d-1\}$ (i.e., leaving out the zeroth index), plotted for various choices of the tolerance ε (cf. (2.5)). The sketch dimension is $n = 2000$ for each curve. The final values of the ESS per sample after the unbiasing step at the end of the reverse diffusion are 0.149, 0.923, and 0.967 for $\varepsilon = 10^{-1}$, 10^{-2} , and 10^{-3} , respectively.

References

- [1] Michael S. Albergo and Eric Vanden-Eijnden. Nets: A non-equilibrium transport sampler, 2025.
- [2] Shun-ichi Amari. *Differential-geometrical methods in statistics*, volume 28. Springer Science & Business Media, 1985.
- [3] Shun-ichi Amari. Natural gradient works efficiently in learning. *Neural computation*, 10(2):251–276, 1998.
- [4] Michael Arbel, Alexander G. D. G. Matthews, and Arnaud Doucet. Annealed flow transport monte carlo. In *Proceedings of the 38th International Conference on Machine Learning*, Proceedings of Machine Learning Research, 18–24 Jul 2021.
- [5] Federico Becca and Sandro Sorella. *Quantum Monte Carlo Approaches for Correlated Systems*. Cambridge University Press, 2017.
- [6] Jules Berman and Benjamin Peherstorfer. Randomized sparse neural galerkin schemes for solving evolution equations with deep networks. In *Proceedings of the 37th International Conference on Neural Information Processing Systems*, NIPS '23, Red Hook, NY, USA, 2023. Curran Associates Inc.
- [7] Michael Betancourt. A conceptual introduction to Hamiltonian Monte Carlo. (arXiv:1701.02434), July 2018. arXiv:1701.02434 [stat].
- [8] Nicholas M Boffi and Eric Vanden-Eijnden. Probability flow solution of the Fokker-Planck equation. *Machine Learning: Science and Technology*, 4(3):035012, jul 2023.
- [9] Nicholas M. Boffi and Eric Vanden-Eijnden. Deep learning probability flows and entropy production rates in active matter. *Proceedings of the National Academy of Sciences*, 121(25):e2318106121, 2024.
- [10] James Bradbury, Roy Frostig, Peter Hawkins, Matthew James Johnson, Chris Leary, Dougal Maclaurin, George Necula, Adam Paszke, Jake VanderPlas, Skye Wanderman-Milne, and Qiao Zhang. JAX: composable transformations of Python+NumPy programs, 2018.
- [11] Joan Bruna, Benjamin Peherstorfer, and Eric Vanden-Eijnden. Neural Galerkin schemes with active learning for high-dimensional evolution equations. *Journal of Computational Physics*, 496:112588, January 2024.
- [12] Ao Chen and Markus Heyl. Empowering deep neural quantum states through efficient optimization. *Nature Physics*, 20(9):1476–1481, 2024.
- [13] Zhuo Chen, Jacob Mccarran, Esteban Vizcaino, Marin Soljagic, and Di Luo. TENG: Time-evolving natural gradient for solving PDEs with deep neural nets toward machine precision. In Ruslan Salakhutdinov, Zico Kolter, Katherine Heller, Adrian Weller, Nuria Oliver, Jonathan Scarlett, and Felix Berkenkamp, editors, *Proceedings of the 41st International Conference on Machine Learning*, volume 235 of *Proceedings of Machine Learning Research*, pages 7143–7162. PMLR, 21–27 Jul 2024.

- [14] Biwei Dai and Uros Seljak. Sliced iterative normalizing flows. In Marina Meila and Tong Zhang, editors, *Proceedings of the 38th International Conference on Machine Learning*, volume 139 of *Proceedings of Machine Learning Research*, pages 2352–2364. PMLR, 18–24 Jul 2021.
- [15] Biwei Dai and Uros Seljak. Translation and rotation equivariant normalizing flow (trenf) for optimal cosmological analysis. *Monthly Notices of the Royal Astronomical Society*, 516(2):2363–2373, 07 2022.
- [16] Biwei Dai and Uros Seljak. Multiscale flow for robust and optimal cosmological analysis. *Proceedings of the National Academy of Sciences*, 121(9):e2309624121, 2024.
- [17] Arnaud Doucet, Will Sussman Grathwohl, Alexander G. D. G. Matthews, and Heiko Strathmann. Score-based diffusion meets annealed importance sampling. In Alice H. Oh, Alekh Agarwal, Danielle Belgrave, and Kyunghyun Cho, editors, *Advances in Neural Information Processing Systems*, 2022.
- [18] Yifan Du and Tamer A. Zaki. Evolutional deep neural network. *Phys. Rev. E*, 104:045303, Oct 2021.
- [19] Michael Feischl, Caroline Lasser, Christian Lubich, and Jorg Nick. Regularized dynamical parametric approximation, 2024.
- [20] Tomas Geffner and Justin Domke. Langevin diffusion variational inference. In Francisco Ruiz, Jennifer Dy, and Jan-Willem van de Meent, editors, *Proceedings of The 26th International Conference on Artificial Intelligence and Statistics*, volume 206 of *Proceedings of Machine Learning Research*, pages 576–593. PMLR, 25–27 Apr 2023.
- [21] Gil Goldshlager, Nilin Abrahamsen, and Lin Lin. A kaczmarsz-inspired approach to accelerate the optimization of neural network wavefunctions. *Journal of Computational Physics*, 516:113351, 2024.
- [22] James Gubernatis, Naoki Kawashima, and Philipp Werner. *Quantum Monte Carlo Methods*. Cambridge University Press, 2016.
- [23] Jonathan Ho, Ajay Jain, and Pieter Abbeel. Denoising diffusion probabilistic models. In H. Larochelle, M. Ranzato, R. Hadsell, M.F. Balcan, and H. Lin, editors, *Advances in Neural Information Processing Systems*, volume 33, pages 6840–6851. Curran Associates, Inc., 2020.
- [24] Jonathan Ho, Chitwan Saharia, William Chan, David J Fleet, Mohammad Norouzi, and Tim Salimans. Cascaded diffusion models for high fidelity image generation. *arXiv preprint arXiv:2106.15282*, 2021.
- [25] Jonathan Ho and Tim Salimans. Classifier-free diffusion guidance. In *NeurIPS 2021 Workshop on Deep Generative Models and Downstream Applications*, 2021.
- [26] Jonathan Ho, Tim Salimans, Alexey Gritsenko, William Chan, Mohammad Norouzi, and David J Fleet. Video diffusion models. *arXiv:2204.03458*, 2022.
- [27] Arthur Jacot, Franck Gabriel, and Clement Hongler. Neural tangent kernel: Convergence and generalization in neural networks. In S. Bengio, H. Wallach, H. Larochelle, K. Grauman, N. Cesa-Bianchi, and R. Garnett, editors, *Advances in Neural Information Processing Systems*, volume 31. Curran Associates, Inc., 2018.

- [28] Minas Karamanis, Florian Beutler, John A Peacock, David Nabergoj, and Uroš Seljak. Accelerating astronomical and cosmological inference with preconditioned monte carlo. *Monthly Notices of the Royal Astronomical Society*, 516(2):1644–1653, 2022.
- [29] Minas Karamanis, David Nabergoj, Florian Beutler, John A Peacock, and Uros Seljak. pocomc: A python package for accelerated bayesian inference in astronomy and cosmology. *arXiv preprint arXiv:2207.05660*, 2022.
- [30] Patrick Kidger. *On Neural Differential Equations*. PhD thesis, University of Oxford, 2021.
- [31] P. Michael Kielstra and Michael Lindsey. A gradient-based and determinant-free framework for fully bayesian gaussian process regression, 2024.
- [32] Diederik Kingma and Jimmy Ba. Adam: A method for stochastic optimization. *International Conference on Learning Representations*, 12 2014.
- [33] Vidhi Lalchand and Carl Edward Rasmussen. Approximate inference for fully bayesian gaussian process regression. In Cheng Zhang, Francisco Ruiz, Thang Bui, Adji Bousso Dieng, and Dawen Liang, editors, *Proceedings of The 2nd Symposium on Advances in Approximate Bayesian Inference*, volume 118 of *Proceedings of Machine Learning Research*, pages 1–12. PMLR, 08 Dec 2020.
- [34] Jun S. Liu. Metropolized independent sampling with comparisons to rejection sampling and importance sampling. *Statistics and Computing*, 6(2):113–119, 1996.
- [35] Per-Gunnar Martinsson and Joel A. Tropp. Randomized numerical linear algebra: Foundations and algorithms. *Acta Numerica*, 29:403–572, 2020.
- [36] Alexander G. D. G. Matthews, Michael Arbel, Danilo J. Rezende, and Arnaud Doucet. Continual repeated annealed flow transport monte carlo. In *Proceedings of the 39th International Conference on Machine Learning*, Proceedings of Machine Learning Research, Jul 2022.
- [37] Riley Murray, James Demmel, Michael W. Mahoney, N. Benjamin Erichson, Maksim Melnichenko, Osman Asif Malik, Laura Grigori, Piotr Luszczek, Michal Dereziński, Miles E. Lopes, Tianyu Liang, Hengrui Luo, and Jack Dongarra. Randomized numerical linear algebra : A perspective on the field with an eye to software, 2023.
- [38] Levon Nurbekyan, Wanzhou Lei, and Yunan Yang. Efficient natural gradient descent methods for large-scale pde-based optimization problems. *SIAM Journal on Scientific Computing*, 45(4):A1621–A1655, 2023.
- [39] M. Raissi, P. Perdikaris, and G. E. Karniadakis. Physics-informed neural networks: A deep learning framework for solving forward and inverse problems involving nonlinear partial differential equations. *Journal of Computational Physics*, 378:686–707, February 2019.
- [40] Carl Edward Rasmussen and Christopher K. I. Williams. *Gaussian processes for machine learning*. Adaptive computation and machine learning. MIT Press, Cambridge, Mass, 2006. OCLC: ocm61285753.
- [41] Hannes Risken. *The Fokker-Planck Equation: Methods of Solution and Applications*, volume 18 of *Springer Series in Synergetics*. Springer, Berlin, Heidelberg, 1996.

- [42] Jascha Sohl-Dickstein, Eric Weiss, Niru Maheswaranathan, and Surya Ganguli. Deep unsupervised learning using nonequilibrium thermodynamics. In Francis Bach and David Blei, editors, *Proceedings of the 32nd International Conference on Machine Learning*, volume 37 of *Proceedings of Machine Learning Research*, pages 2256–2265, Lille, France, 07–09 Jul 2015. PMLR.
- [43] Yang Song, Jascha Sohl-Dickstein, Diederik P Kingma, Abhishek Kumar, Stefano Ermon, and Ben Poole. Score-based generative modeling through stochastic differential equations. In *International Conference on Learning Representations*, 2021.
- [44] Yifeng Tian, Nishant Panda, and Yen Ting Lin. Liouville flow importance sampler. In *Proceedings of the 41st International Conference on Machine Learning, ICML’24*. JMLR.org, 2024.
- [45] Ch. Tsitouras. Runge-kutta pairs of order 5(4) satisfying only the first column simplifying assumption. *Comput. Math. Appl.*, 62(2):770–775, July 2011.
- [46] Francisco Vargas, Will Sussman Grathwohl, and Arnaud Doucet. Denoising diffusion samplers. In *The Eleventh International Conference on Learning Representations*, 2023.
- [47] Yuxiao Wen, Eric Vanden-Eijnden, and Benjamin Peherstorfer. Coupling parameter and particle dynamics for adaptive sampling in neural galerkin schemes. *Physica D: Nonlinear Phenomena*, 462:134129, 2024.
- [48] Hao Wu, Jonas Köhler, and Frank Noe. Stochastic normalizing flows. In H. Larochelle, M. Ranzato, R. Hadsell, M.F. Balcan, and H. Lin, editors, *Advances in Neural Information Processing Systems*, volume 33, pages 5933–5944. Curran Associates, Inc., 2020.
- [49] Huan Zhang, Yifan Chen, Eric Vanden-Eijnden, and Benjamin Peherstorfer. Sequential-in-time training of nonlinear parametrizations for solving time-dependent partial differential equations, 2024.